

Fragile morphotropic phase boundary and phase stability in the near-surface region of the relaxor ferroelectric $(1-x)\text{Pb}(\text{Zn}_{1/3}\text{Nb}_{2/3})\text{O}_3-x\text{PbTiO}_3$: [001] field-cooled phase diagrams

Yaojin Wang (汪尧进)^{1,2,*} Ding Wang,¹ Guoliang Yuan,¹ He Ma,¹ Feng Xu,¹ Jiefang Li,² D. Viehland,² and Peter M. Gehring³

¹*School of Materials Science and Engineering, Nanjing University of Science and Technology, Nanjing 210094, Jiangsu, China*

²*Materials Science and Engineering, Virginia Tech, Blacksburg, Virginia 24061, USA*

³*NIST Center for Neutron Research, National Institute of Standards and Technology, Gaithersburg, Maryland 20899-6100, USA*

(Received 24 April 2014; revised manuscript received 15 August 2016; published 10 November 2016)

We have examined the effects of field cooling on the phase diagram of the relaxor system $(1-x)\text{Pb}(\text{Zn}_{1/3}\text{Nb}_{2/3})\text{O}_3-x\text{PbTiO}_3$ (PZN- x PT) for compositions near the morphotropic phase boundary (MPB). High-resolution diffraction measurements using Cu K_α x rays, which probe $\approx 3 \mu\text{m}$ below the crystal surface, were made on field-cooled (FC) single-crystal specimens of PZN-4.5%PT and PZN-6.5%PT under electric fields of 1 and 2 kV/cm applied along [001] and combined with previous neutron diffraction data, which probe the entire crystal volume, for FC PZN-8%PT [Ohwada *et al.*, *Phys. Rev. B* **67**, 094111 (2003)]. A comparison to the zero-field-cooled (ZFC) PZN- x PT phase diagram reveals several interesting features: (1) The short-range monoclinic phase observed in the ZFC state on the low-PT side of the MPB is replaced by a monoclinic M_A phase; (2) field cooling extends the tetragonal phase to higher temperatures and lower-PT concentrations; (3) the orthorhombic phase near the MPB is replaced by a monoclinic M_C phase; (4) the vertical MPB in the ZFC phase diagram bends significantly towards the low-PT side in the FC state. These results demonstrate that both the phase stability and the nature of the MPB in PZN-PT within the near-surface regions are fragile in the presence of electric fields.

DOI: [10.1103/PhysRevB.94.174103](https://doi.org/10.1103/PhysRevB.94.174103)

I. INTRODUCTION

Piezoelectrics are materials that convert mechanical energy to electrical energy and vice versa. They are thus of significant importance to medical ultrasound, actuators, sensors, and countless other device applications [1–3]. Among such materials, solid solutions of the complex perovskites $\text{Pb}(\text{Zn}_{1/3}\text{Nb}_{2/3})\text{O}_3$ and $\text{Pb}(\text{Mg}_{1/3}\text{Nb}_{2/3})\text{O}_3$ with PbTiO_3 (denoted PZN- x PT and PMN- x PT, respectively, where x indicates the atomic percentage of Ti) are relaxor ferroelectrics that exhibit exceptional piezoelectric properties [2]. In particular, extraordinarily high values of the longitudinal piezoelectric coefficient d_{33} have been reported for PZN-8%PT when an electric field (E) is applied along the pseudocubic [001] direction, reaching values of 2500 pC/N and induced strains $\varepsilon \geq 1.7\%$ [2,4]. These values are nearly one order of magnitude larger than those observed for conventional piezoelectric ceramics such as $\text{Pb}(\text{Zr}_x\text{Ti}_{1-x})\text{O}_3$ (PZT). Yet PMN- x PT, PZN- x PT, and PZT have qualitatively similar temperature-composition phase diagrams: The high-temperature paraelectric phases are all cubic (C , space group $Pm\bar{3}m$), and the low-temperature ferroelectric phases are rhombohedral (R , space group $R3m$) for low x and tetragonal (T , space group $P4mm$) at higher x [5–7]. The strong piezoelectric properties of these materials have been associated with a very steep morphotropic phase boundary (MPB) that separates the T and R phases [5,6,8]. For this reason, many diffraction studies have been performed with excellent wave vector (q) resolution to try to identify the low-symmetry phase located closest to the MPB on the rhombohedral side and to determine the extent of its stability.

In PZT, monoclinic $Cm A$ (M_A) and $Cm B$ (M_B) phases have been reported that bridge the R and T phases near the

MPB for $46\% \leq x \leq 52\%$ [9–11]. The M_A and M_B phases have a unique axis b_m that lies along the [110] direction; the unit cell is doubled and rotated 45° about the c axis with respect to the primitive C cell [12]. In PMN- x PT, however, the MPB region is also complicated. Monoclinic $Pm C$ (M_C) and M_B phases coexist with R , T , and orthorhombic $Amm2$ (O) phases for $30\% \leq x \leq 37\%$ [5,13]. The M_C phase has a primitive unit cell, with a unique axis b_m oriented along [010]. For PZN- x PT, the existence of an O phase for $9\% \leq x \leq 11\%$ has been reported between the R and T phases [6]. The O phase in BaTiO_3 can be viewed as a limiting case of the monoclinic M_C phase with $a_m = c_m$ [14]. Uesu *et al.* also observed an M_C phase (i.e., $a_m \neq c_m$) in the ground state of one PZN-9%PT crystal; however, two others exhibited a stable O phase [15]. Since the seminal discovery of an intermediate monoclinic phase in PZT [10,16], the zero-field-cooled (ZFC) temperature-composition phase diagrams of these other lead-oxide perovskite ferroelectric relaxors have been revised [5,6,10,11,13].

Generally, an applied electric field will alter the free-energy landscape and thus the various possible polar phases in the vicinity of the MPB [17]. Recently, Ma *et al.* [18] reported that the MPB of annealed, lead-free $(\text{Bi}_{1/2}\text{Na}_{1/2})\text{TiO}_3$ - BaTiO_3 can be created, destroyed, or even replaced by another MPB via phase transitions induced by poling. Moreover, Cao *et al.* [19] have constructed field-cooled (FC) temperature-composition phase diagrams for PMN- x PT for E applied parallel to [001] and [110]. These FC diagrams revealed two interesting features: (i) the presence of a pseudocubic region of abnormal thermal expansion ($c \neq a$) above the dielectric maximum, where the stability range extends to higher temperatures than in the ZFC state; and (ii) a change in the shape of the MPB in the FC state; i.e., the stability of the T phase is extended to $x = 0.25$ in the [001] FC state, and it is replaced by an O phase

*yjwang@njust.edu.cn

in the [110] FC state [19]. In a neutron study of PZN-8%PT, Ohwada *et al.* [20] reported the phase transition sequence $C \rightarrow T \rightarrow M_C$ on cooling from 550 to 300 K in an electric field $E \parallel [001]$. They also found that the $C \rightarrow T$ Curie temperature (T_C) in the FC state is ~ 20 K higher (when $E = 2$ kV/cm) than that in the ZFC state, and that the R phase of the ZFC state is replaced by M_C [6,20]. Several neutron and x-ray diffraction studies have been performed to determine the origin of the high piezoelectricity in PZN- x PT by gradually increasing E at fixed temperature, thereby providing a link between the piezoelectric properties and the structural parameters [5,20,21]. However, the underlying mechanism(s) cannot be fully understood without first understanding the evolution of the MPB in the FC state.

In this paper, we report the results of an x-ray diffraction (XRD) study performed with high resolution on single-crystal PZN- x PT compositions located near the MPB in both ZFC and FC states. Our findings are summarized in Fig. 1. The open and solid circles represent data reported previously by Kuwata *et al.* [22] and La-Orauttapong *et al.* [6], respectively. The vertical dotted lines and the shaded region represent the MPB in the ZFC state. The solid squares represent the phase transition temperatures we measured using XRD in the FC state with $E = 1$ kV/cm $\parallel [001]$ together with those previously reported by Ohwada *et al.* [20] (shaded circles). The modified phase diagram demonstrates that the MPB is quite fragile, and can be either destroyed or reconfigured/created

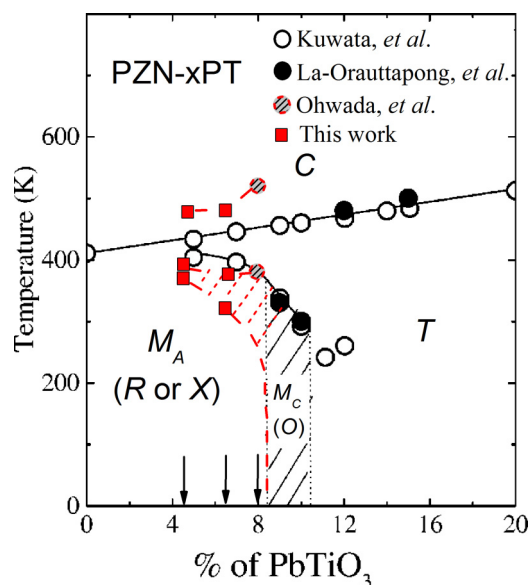


FIG. 1. PZN- x PT phase diagram near the MPB. Open circles represent the data for ZFC PZN- x PT reported by Kuwata *et al.* [22]. Solid circles represent the more recent data for ZFC PZN- x PT reported by La-Orauttapong *et al.* [6]. The symbols R (or X) and O designate the rhombohedral (or X) and orthorhombic ZFC phases. Our x-ray data on FC PZN-4.5%PT and PZN-6.5%PT are plotted as solid squares and included with the neutron data of Ohwada *et al.* for FC PZN-8%PT (shaded circles). The black dotted lines represent the MPB in the ZFC state, while the red dashed lines represent the MPB in the FC state ($E = 1$ kV/cm $\parallel [001]$). Our ZFC results are not shown in this figure (see text), as they agree well with the ZFC results of La-Orauttapong *et al.* [6].

by application of $E \parallel [001]$. The phase diagram also shows that the stability of the T phase is significantly extended in temperature by an applied electric field E , and the phase transformation sequences and temperatures are discussed within that context.

II. EXPERIMENTAL DETAILS

Single crystals of PZN-4.5%PT and PZN-6.5%PT (provided by Microfine Materials Tech, Singapore) with dimensions of $2 \times 2 \times 4$ mm³ and $2 \times 0.2 \times 4$ mm³, respectively, were cut with $\{100\}$ faces, and all faces were polished to $0.25 \mu\text{m}$. Gold electrodes were deposited on the largest top and bottom surfaces, which we designate as (001) faces. Additionally, ferroelectric (nonrelaxor) single crystals of PMN-60%PT and BaTiO₃ (Shanghai Institute of Ceramics) with dimensions of $3 \times 3 \times 0.5$ mm³ were prepared with the large surface normal oriented along $[001]$ and polished to $0.25 \mu\text{m}$ for use in a contrast experiment. Diffraction measurements were then performed with the scattering vector \mathbf{Q} oriented along $[001]$. Diffraction measurements were also performed along $[H00]$ and $[HH0]$ on the PZN-4.5%PT crystals. For the PZN-6.5%PT crystals, however, after finishing the measurements along $[00L]$ the electrodes were removed using a polishing blanket with $0.25\text{-}\mu\text{m}$ aluminum powder; new electrodes were then created by applying silver paint to one pair of opposing faces perpendicular to the original (001) faces. Diffraction measurements were then performed using a Philips MPD high-resolution system, which is shown schematically in Fig. 2(a). An incident monochromatic x-ray beam was produced by a line-focus x-ray source together with a two-bounce hybrid monochromator using Ge (220) crystals.

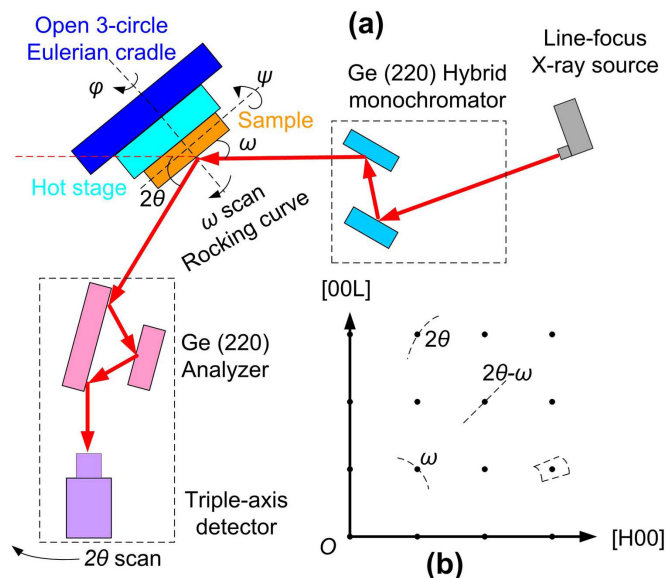


FIG. 2. Schematic diagram of (a) the Philips MPD high-resolution x-ray diffractometer and (b) single- and reciprocal-space mesh scans in the (HOL) zone. The rocking curve (ω scan) describes a circular arc centered on the origin, the detector scan (2θ scan) follows the circumference of the Ewald sphere, and the ω - 2θ radial scan describes a straight line pointing radially from the origin. A typical reciprocal-space mesh scan centered on $(301)_C$ is shown.

The system was equipped with an open three-circle Eulerian cradle, which enabled samples to be rotated (φ movement), tilted (ψ movement), and rocked (ω scans). A domed hot stage was mounted on the cradle, and the temperature was computer controlled. A Ge (220) cut crystal was used as an analyzer in which the diffracted beam undergoes three reflections within the groove before entering the detector. The x-ray beam size was chosen to be $3 \times 3 \text{ mm}^2$, and the wavelength was that of $\text{Cu } K_{\alpha} = 1.5406 \text{ \AA}$. The x-ray generator was operated at 45 kV and 40 mA. Under these conditions, the instrumental wave vector resolution at (200) is 0.0068° in 2θ full width at half maximum (FWHM). The lattice parameters were obtained from radial (ω - 2θ) scans measured across the (002), (200), and (220) Bragg peaks. All of these scans were performed using an angular step size of 0.002° and an integration time of 2 s. To determine the domain configurations, reciprocal-space mesh scans (RMSs) were measured around the (002) and (200) or (020) Bragg peaks in the ($H0L$) or ($0HL$) zones, and around (220) in the (HHL) zone. These were generated by performing a sequence of ω - 2θ scans at different ω offsets using a step size of 0.01° with an integration time of 0.5 s [see Fig. 2(b)] and are shown as intensity as a function of reciprocal lattice position. Each measurement cycle began by heating to 600 K to anneal the crystals in order to decrease the internal strain [23]; measurements were subsequently taken on cooling. At 520 K, the cubic lattice constant for PZN-6.5%PT is $a = 4.054 \text{ \AA}$; the corresponding cubic reciprocal lattice unit (or rlu) is $a^* = 2\pi/a = 1.550 \text{ \AA}^{-1}$. All reciprocal-space mesh scans shown here are plotted in reciprocal lattice units.

We note that the x-ray penetration depth ($1/e$) due to absorption in these PZN- x PT crystals at (200) is only $\sim 2.6 \mu\text{m}$ [24], thus our diffraction measurements probe only the near-surface region. Normally, this is more than sufficient to determine the bulk structure of most materials. However, this is not the case for relaxors. An anomalous skin effect spanning the top most 50 to 100 μm of the crystal surface has been reported in single crystals of PZN- x PT, PMN- x PT, and $\text{Na}_{1/2}\text{Bi}_{1/2}\text{TiO}_3$ (NBT) in which the near-surface crystal structure differs from that of the bulk [25–27]. This is an extremely important point because the small x-ray penetration depth means that the majority of the x rays scatter from just the first one or two microns of the crystal surface, and this will produce variability in the diffraction peak profiles and lattice parameters. We will discuss this issue further in the following sections.

In order to investigate the surface domain configuration of PZN- x PT, piezoresponse force microscope (PFM) measurements were also performed using an atomic force microscope (AFM, Bruker multimode 8) with an open loop controller and a conductive AFM tip (MESP-RC, Co/Cr coating, 35-nm tip radius) under contact mode. Temperature control between 300 and 520 K was obtained using a Bruker Multimode heater stage with an accuracy of 0.5°C .

III. PHASE TRANSITIONS, LATTICE PARAMETERS, AND PHASE DIAGRAMS

Figure 1 displays the composition-temperature phase diagram for both ZFC and FC ($E = 1 \text{ kV/cm}$) conditions and summarizes the main results of this study. To obtain a more detailed picture of how the phase transitions in PZN- x PT

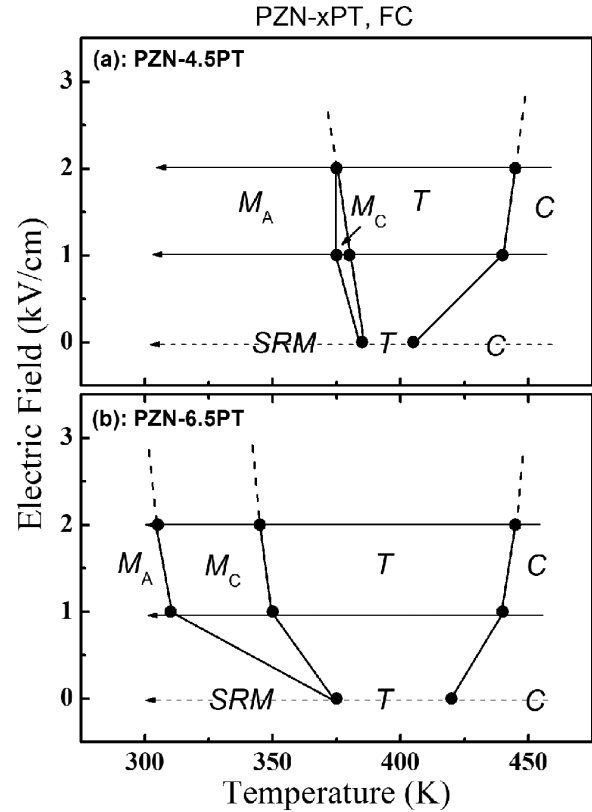


FIG. 3. Electric field-temperature phase diagram for (a) PZN-4.5%PT and (b) PZN-6.5%PT in the FC state with $E \parallel [001]$. Arrows indicate the sequence of phase transitions on cooling. Solid circles represent the respective transition temperatures as defined in the text. Lines are guides to the eyes.

are affected by an electric field, x-ray measurements were performed on cooling under electric fields of $E = 0, 1,$ and 2 kV/cm applied parallel to $[001]$. The resulting electric field-temperature phase diagrams determined for PZN-4.5%PT and PZN-6.5%PT are summarized in Fig. 3. The transition temperatures were determined by following the evolution of the lattice parameters and peak profiles. Details of the XRD measurements and data analysis are given in the next sections.

A. Phase transitions and lattice parameters in ZFC PZN- x PT

The ZFC lattice parameters were measured by heating the crystal to 600 K, annealing for 30 min, and then performing radial scans through the pseudocubic (200) and (220) Bragg peaks on cooling. Data from scans measured at five different temperatures are shown in Fig. 4 for PZN-4.5%PT. Two surprising features are immediately evident: (1) The Bragg peak profiles are asymmetric in the cubic phase, particularly for (200); and (2) the Bragg peaks broaden markedly on cooling into the purported T phase. The peak asymmetry is unexpected because it is absent in radial scans measured using the identical x-ray setup in the cubic phases of single-crystal specimens of BaTiO_3 and PMN-60%PT, neither of which is a relaxor (see Fig. 11). The asymmetry is therefore a real effect and indicates the presence of a significant lattice gradient (strain) within the near-surface region of the relaxor ferroelectric crystals. This finding is consistent with the previous studies of the anomalous

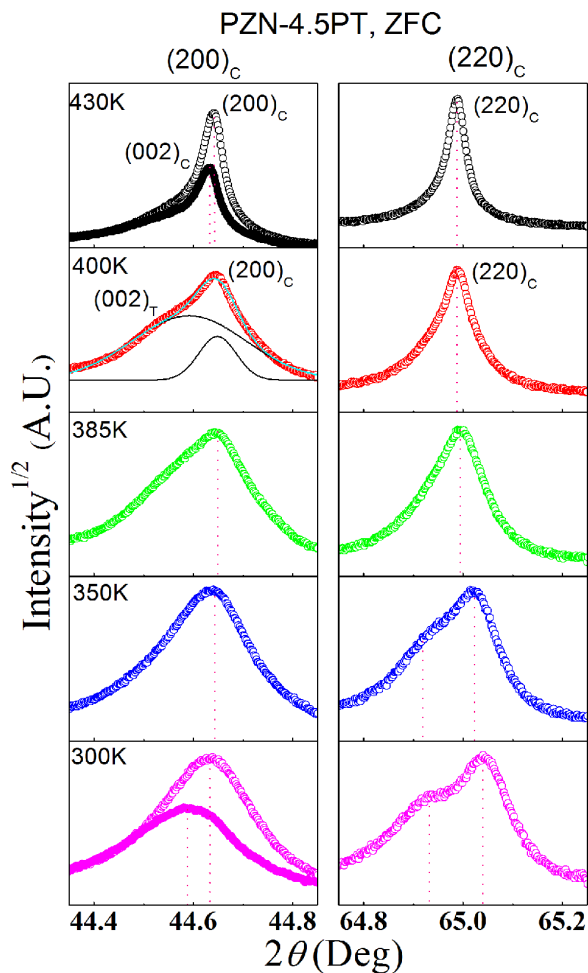


FIG. 4. Evolution of the pseudocubic $(200)_C$ and $(220)_C$ Bragg peak line shapes on cooling from the cubic phase to the short-range-ordered monoclinic phase for PZN-4.5%PT. Open and solid circles represent the $(200)_C$ and $(002)_C$ peak profiles in the C and short-range-ordered monoclinic phases, respectively. The square root of the diffracted x-ray intensity is plotted in order to make weak peaks and shoulders more visible.

skin effect in PZN- x PT [23] and PMN- x PT [26] mentioned earlier. In particular, the neutron study by Conlon *et al.* on pure PMN found that the lattice parameter varies as a function of depth measured from the crystal surface over a range of order $100 \mu\text{m}$ [28]. The broadening of the Bragg peaks on cooling is equally unexpected because it indicates that no long-range-ordered (LRO) phase transitions take place in this material in the ZFC state over this temperature range within the crystal volume probed by the x-ray beam. The broadening of the Bragg peaks is discussed in Sec. IV.

For PZN-4.5%PT, evidence of a short-range-ordered T -like phase is apparent near 420 K from the fit to two broad Gaussian peaks shown in the left column of Fig. 4 at 400 K. On further cooling, a continued coexistence of C - and T -like phases is observed until a transition into a different structure occurs near 380 K. Interestingly, PZN-4.5%PT exhibits a T -like phase only in the presence of a coexisting C phase. The a domains of the T -like phase are not apparent in the (002) zone. The tetragonal c -domain nucleation and growth in the C phase has also been observed in a generation of

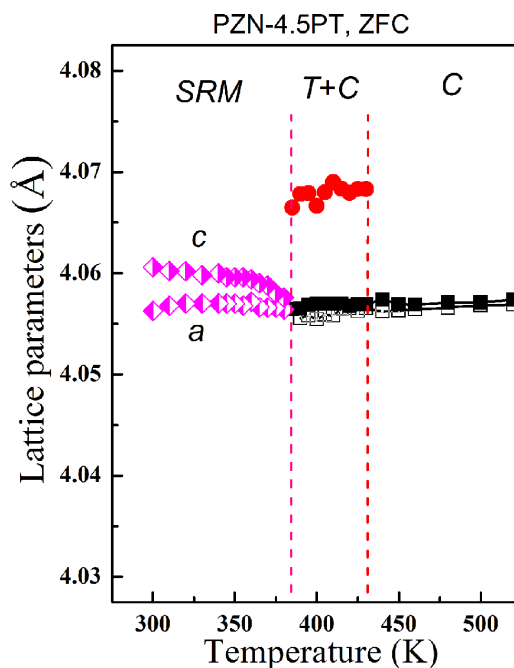


FIG. 5. Lattice parameters of ZFC PZN-4.5%PT as a function of temperature.

relaxor ferroelectric single crystals [29], where the tetragonal a domains were observed only on further cooling. The T -like diffraction features are discussed in Sec. IV (see Fig. 10). The c -axis lattice parameter for the T -like phase is shown in Fig. 5, but the a -axis lattice parameter could not be determined. Ohwada *et al.* performed neutron diffraction measurements on PZN-8%PT and concluded that the ZFC structure at low temperature is not R [20], as had previously been accepted [6]. Subsequent high-energy x-ray studies by Xu *et al.* on PZN [26], and high-resolution neutron studies by Gehring *et al.* [30] on PMN-10%PT, also showed that the low-temperature bulk phase is not R . As the true ground-state bulk crystal symmetry was unknown, the bulk phase was named phase X , which designates a distorted structure within an average cubic phase [20].

According to the accepted zero-field PZN- x PT phase diagram [6,22], one expects a transition to a LRO R phase for PZN-4.5%PT below ~ 400 K. Assuming a multidomain sample, this should manifest itself as a narrow single peak at (200) and two sharp peaks at (220) . However, from Fig. 4 we see that at 385 K the pseudocubic (200) peak profile remains extremely broad and continues to exhibit a weak, secondary peak on the low-angle side, both of which are inconsistent with a LRO R phase. But on cooling to 350 K and then to 300 K the (200) peak profile becomes increasingly better described by a single broad peak. At the same time, the (220) peak profile gradually exhibits an increasingly stronger peak splitting, although it too remains very broad. These data are thus consistent with the gradual formation of a short-range-ordered (SRO) R phase that is limited to the near-surface region in PZN-4.5%PT, which matches the conclusions of Xu *et al.* [25], who observed a SRO R phase in the near-surface region of PZN-4.5%PT using 10.2-keV x rays, but a less-distorted (smaller rhombohedral angle) R phase using 67-keV x rays,

which penetrate much deeper into the crystal. The behavior in Fig. 4 is also reminiscent of the x-ray diffraction study of single-crystal PZN by Lebon *et al.* [31] who observed that the $C \rightarrow R$ transition occurs gradually between 385 and 325 K and could be described by the formation of nanometer-sized R domains that grow in number, but not in size, on cooling, thus leading to very broad x-ray diffraction peak profiles.

We also performed radial scans at (002); these are shown in the bottom panel (300 K) on the left-hand column in Fig. 4. It can be seen that the positions of the $(200)_C$ and $(002)_C$ Bragg peaks do not coincide, whereas above 430 K they nearly do. This is possibly due to the presence of a different surface strain between (200) and (002), which correspond to different faces of the same crystal, or to an undetermined phase in the near-surface region of the relaxors. The resulting lattice parameters, shown in Fig. 5, were determined by analyzing the (200) and (002) peak line shapes. The c -axis lattice parameter increases and the a -axis lattice parameter decreases on cooling, which matches the temperature evolution of the T lattice parameters. Further details regarding this analysis are provided in Sec. IV. Similar results were obtained for PZN-6.5%PT (data not shown), and the phase transition temperatures agreed well with those of the accepted ZFC phase diagram [6,22].

B. Phase transitions in [001] FC PZN- x PT

We now discuss the effects of an electric field on the sequence of phase transitions in PZN- x PT in the FC state. The crystals were initially annealed at 600 K after which fields of $E = 1$ and 2 kV/cm were successively applied parallel to [001]. The phase transformational sequence in the FC state was then studied on cooling by conducting radial and reciprocal-space mesh scans performed close to the pseudocubic (002), (200), and (220) Bragg peaks.

For PZN-4.5%PT under $E = 1$ kV/cm, the phase transformational sequence is $C \rightarrow T \rightarrow M_C \rightarrow M_A$, where the M_C phase coexists with the T phase over a narrow temperature range. At $E = 2$ kV/cm, the transformational sequence is $C \rightarrow T \rightarrow M_A$. The difference in these two sequences indicates that the left side of the MPB in the FC state is located near $x = 4.5$ for moderate E field strengths. Figure 6 shows the evolution of the pseudocubic (200) Bragg peak profiles with temperature for (a) $E = 1$ kV/cm and (b) 2 kV/cm. At high temperatures, the system is cubic, thus the (200) peak is not split, but the lattice parameter determined from (002) radial scans (data not shown) is always slightly larger than that determined from (200) radial scans [see Fig. 9(a)]. On cooling, the crystal structure transforms to T near 440 K for $E = 1$ kV/cm and 445 K for $E = 2$ kV/cm. However no T -related splitting of either the (200) or (002) Bragg peaks was observed ostensibly because the field-cooling process produced a predominantly single-domain state. This is evident from the reciprocal-space mesh scans shown in Figs. 7(a)–7(c). For this reason, the c - and a -axis lattice parameters were determined from radial scans performed at (002) and (200), respectively. The thermal variation of the lattice parameters is shown in Fig. 9(a).

At 380 K and $E = 1$ kV/cm, the crystal adopts an M_C (b domain) phase, which coexists with the T phase. This conclusion is supported by the presence of two peaks in the

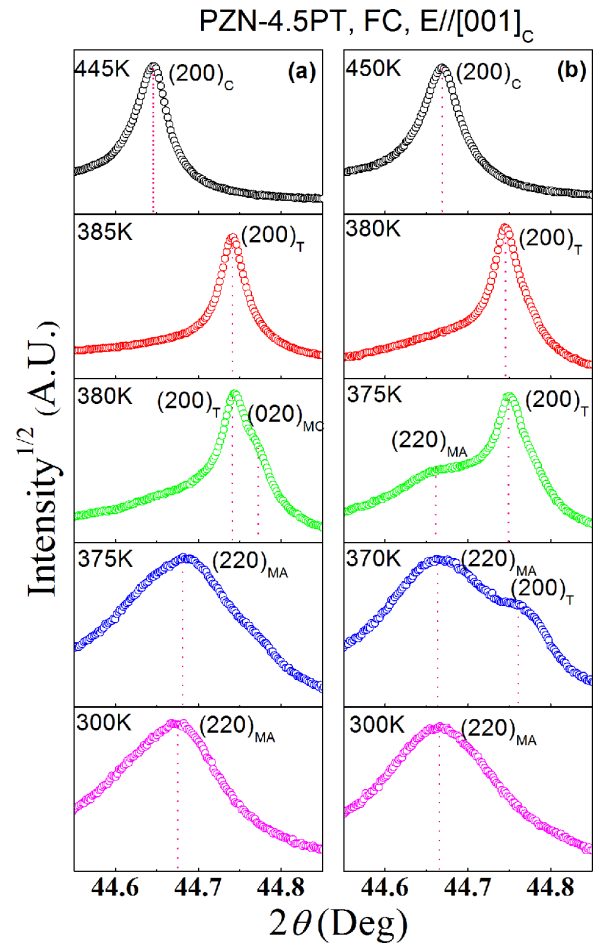


FIG. 6. Evolution of the pseudocubic (200) Bragg peaks for PZN-4.5%PT cooled under (a) $E = 1$ kV/cm and (b) $E = 2$ kV/cm, respectively, where $E \parallel [001]$. The square root of the diffracted x-ray intensity is plotted in order to make weak peaks and shoulders more visible.

mesh scan at (220) shown in Fig. 7(f). A tendency of the transverse scan at (200) to split was also observed, even though the contour maps shown in Figs. 7(d) and 7(e) around (002) and (200) appear to be single peaks. This is presumed to be due to a small volume fraction of M_C . Interestingly, when the sample is heated back up to 600 K and the electric field is increased to 2 kV/cm, no evidence of an M_C phase is observed in the mesh scan at (200) and (220) (data not shown). The observation of an M_C (b domain) phase under $E = 1$ kV/cm implies that the left side of the MPB in the FC state is located near $x = 4.5$, as shown in Fig. 1. The disappearance of the M_C b domains when $E = 2$ kV/cm demonstrates that the MPB is fragile because it changes dramatically in the presence of relatively weak electric fields. At the same time, the T phase becomes increasingly stable with increasing $E \parallel [001]$. We note here that the M_C phase component was indexed following the phase transformational sequence of the PZN-6.5%PT crystals, but that it was difficult to determine in PZN-4.5%PT.

On further cooling, an M_A phase appears near 375 K for both $E = 1$ kV/cm and 2 kV/cm, as shown in Fig. 6. The appearance of the M_A phase is evident in the reciprocal-space mesh scans [see Figs. 7(g)–7(i)]. The contour maps exhibited a single peak around the (002) zone, revealing that the c

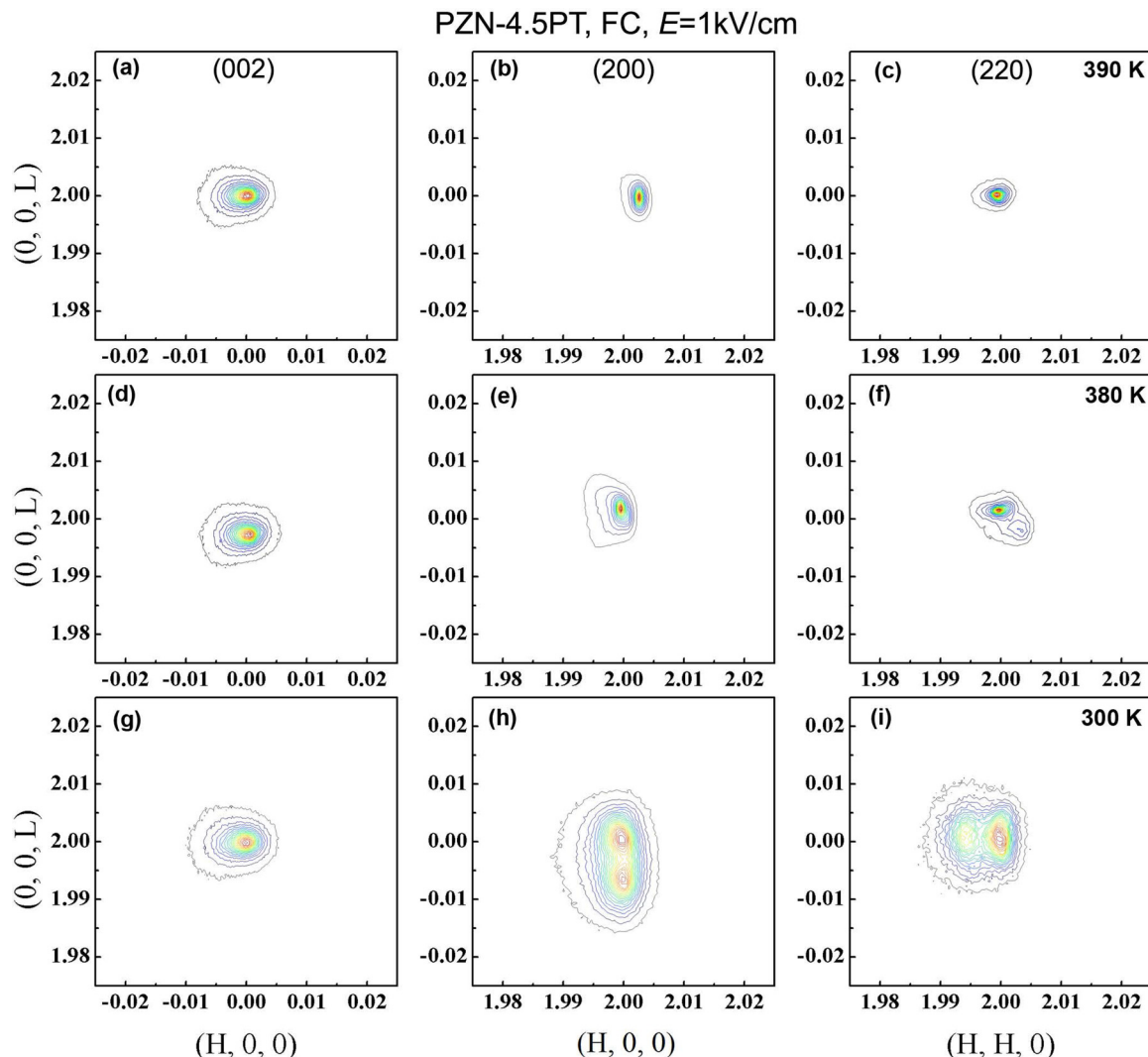


FIG. 7. Reciprocal-space mesh scans centered on the pseudocubic (002), (200), and (220) Bragg peaks at (a)–(c) 390 K, (d)–(f) 380 K and (g)–(i) 300 K for FC PZN-4.5%PT ($E = 1\text{ kV/cm} \parallel [001]$).

axis is fixed along the direction that E is applied. The (200) peak exhibits a splitting along the transverse direction, i.e., (220) – ($\bar{2}20$) twin peaks. These are the signatures of the M_A domain configuration. However, the contour map around (220) does not reveal the signature triplet splitting of the M_A phase (i.e., one b domain, containing two a domains) [19,32], as shown in Fig. 7(i); instead one b domain and a single a domain were apparent. This difference might be related to defects in the crystals.

For PZN-6.5%PT, a phase transition sequence of $C \rightarrow T \rightarrow M_C \rightarrow M_A$ is found in the FC state, similar to that for $x = 4.5\%$. However, in this case the M_C phase is stable over a wider temperature range. For $E = 1\text{ kV/cm}$, the (002)_C peak disappears with decreasing temperature near 440 K and a (200)_T peak develops, demonstrating a $C \rightarrow T$ transformation. Reciprocal-space mesh scans reveal a single-domain configuration for the T phase [see Figs. 8(a)–8(c)]. On cooling to 350 K, a $T \rightarrow M_C$ phase transition is found [see Figs. 8(d)–8(f)]. The pseudocubic (220) peak splits into two peaks along the transverse direction, whereas, the (002) remains a single peak. Interestingly, a single domain is

observed around (200) and (020), which is discussed in detail in Sec. IV. The M_C symmetry is also evident in the temperature evolution of the lattice parameters [see Fig. 9(b)]. The b -axis lattice parameter in the M_C phase decreases continuously with temperature following the a -axis parameter in the T phase [32]. In the ZFC state, it is worth noting that the MPB lies over a narrow compositional range of $9\% < x < 11\%$. However, in the FC state, the M_C phase was clearly present near $x = 6.5\%$ over a wide temperature range. This difference demonstrates that the application of an electric field along [001] bends the MPB over towards the low-PT side of the phase diagram.

A third transition to an M_A phase is observed on cooling to 310 K. As shown in Figs. 8(g)–8(i), the pseudocubic (200) peak splits into two peaks along the transverse direction [i.e., (220) – ($\bar{2}20$) twin peaks]; the (220) peak splits into three peaks [i.e., one b -domain (020) peak and two a -domain (200) – (200) peaks]; and the (002) peak remains a single peak with the c axis fixed by the direction along which E is applied. This domain configuration is well described by the M_A cell in which a_m and b_m lie along the tetragonal $[\bar{1}\bar{1}0]$ and $[1\bar{1}0]$ directions, and c_m is close to the [001] axis [16].

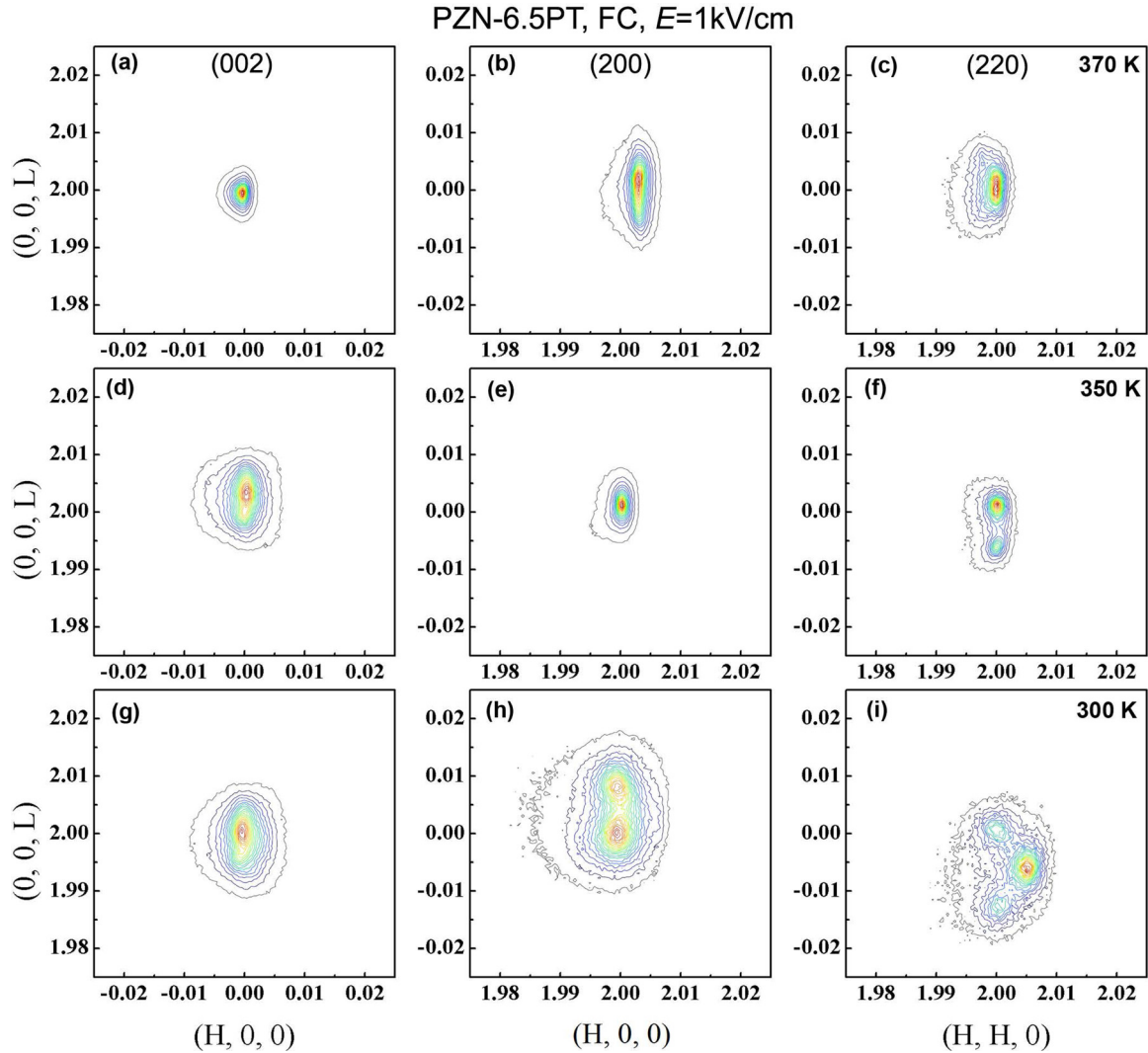


FIG. 8. Reciprocal-space mesh scans centered on the pseudocubic (002), (200), and (220) Bragg peaks at (a)–(c) 370 K, (d)–(f) 350 K and (g)–(i) 300 K for FC PZN-6.5%PT ($E = 1\text{ kV/cm} \parallel [001]$).

C. Lattice parameters for [001] FC PZN- x PT

To clarify the effects of an electric field on the phase transition sequence in PZN- x PT, the temperature dependences of the lattice parameters for both PZN-4.5%PT and PZN-6.5%PT crystals in the FC state for $E = 1\text{ kV/cm}$ are shown in Fig. 9. The cubic lattice parameters for both compositions were determined from radial scans measured at (002) and (200). It can be seen that the values agree well with each other. The tetragonal lattice parameters (a_T , c_T) were extracted from the (200)_T and (002)_T peaks, respectively, and cross checked with scans measured at (220)_T. As expected, the tetragonality ($c/a - 1$) becomes more pronounced with decreasing temperature.

Because only one of the b domains in the M_C phase is observed for PZN-4.5%PT, not all of the lattice parameters could be determined [see Fig. 9(a)]. For PZN-6.5%PT the (002)_T peak abruptly shifts to higher 2θ values at 350 K, indicating that the c axis contracts at the $T \rightarrow M_C$ transition, whereas the (200)_T peak remains a single peak, corresponding to the b domain (020)_{MC}, and shifts continuously to higher 2θ

values with decreasing temperature [see Fig. 9(b)]. The (220)_T peak splits into two peaks along the transverse direction: (220) – ($\bar{2}20$) twin peaks, from which the values of a_m and the monoclinic angle β_C can be extracted.

On cooling to 300 K, both PZN-4.5%PT and PZN-6.5%PT transform into the M_A phase. The c -axis lattice parameter in the M_A phase was calculated from the pseudocubic (002) radial scans and the monoclinic angle β_A . The lattice parameters a_M and b_M were extracted from (220) radial scans. For PZN-4.5%PT, the b -axis lattice parameter of the M_A phase exhibits a discontinuous change at the transition, which was unlike that for PMN-PT, where $b_M/\sqrt{2}$ and a_T continuously decrease with decreasing temperature [33].

IV. DISCUSSION

The study of the ground state and the diffraction peak profiles in relaxors in the ZFC state using x-ray diffraction methods began with our attempts to study the phase transitions and MPB in the FC state. During these measurements, we

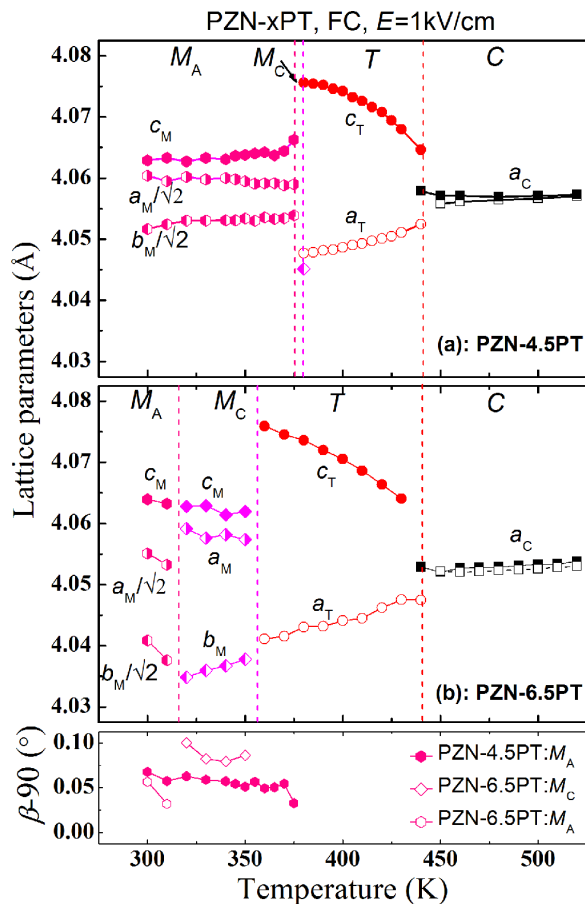


FIG. 9. Lattice parameters of FC (a) PZN-4.5%PT and (b) PZN-6.5%PT as a function of temperature ($E = 1$ kV/cm \parallel [001]). Dashed lines represent the respective transition temperatures as defined in the text. The experimental uncertainties of the lattice parameters extracted from $(002)_C$ and $(200)_C$ are less than 0.001 Å.

noted a significant asymmetry in the diffraction profiles in the cubic phase near the Curie temperature in the ZFC state. As shown in Fig. 4, the $(200)_C$ and $(002)_C$ Bragg peaks always exhibit an asymmetric line shape, even at temperatures well above the Curie temperature. This asymmetry is well described by a very broad peak at low 2θ that coexists with a sharp peak at higher 2θ , and it increases on cooling towards the purported $C \rightarrow T$ transition temperature. Both of these observations can be understood by the existence of a near-surface region, or “skin,” of the crystal that has a depth-dependent lattice spacing, i.e., a lattice gradient that spans at least several microns, which is consistent with the anomalous relaxor skin effect [34]. A comparison of the ZFC and [001] FC diagrams of PZN- x PT in Fig. 1 reveals several interesting findings: (i) that the initial R (or M) phase of the ZFC state is replaced by an M_A phase in the FC state; (ii) that the initial O phase in the ZFC state is replaced by an M_C phase in the FC state; (iii) that the MPB in the ZFC diagram, which is nearly vertical and located near $8\% < x < 11\%$, is destroyed/created in the FC state by modest fields of $E = 1$ and 2 kV/cm; and (iv) that the stability of the T phase is extended to lower-PT compositions and higher temperatures by the application of an electric field.

A. Asymmetric diffraction profiles and phase coexistence at high temperature

1. Near the Curie temperature in the ZFC state

Figure 10(a) shows the temperature dependence of the $(002)_C$ Bragg peak profile for ZFC PZN-4.5%PT. One can see that the peak intensity decreases and the peak width broadens substantially near 420 K. Figure 10(b) shows representative diffraction peak profiles at 500, 400, and 300 K. A fit of the $(002)_C$ Bragg peak at 500 K to a single Gaussian function shows that the profile is not symmetric: It exhibits a weak shoulder on the low-angle side, which is consistent with the presence of a near-surface lattice gradient as reported by Conlon *et al.* [28]. This asymmetry becomes far more pronounced at 420 K. Therefore, below 420 K, the $(002)_C$ peak profiles were fit using two Gaussian peaks to test the possibility that the low-angle shoulder might be the result of a coexistence of a weak (low volume fraction) T phase and a strong C phase. However, on cooling to 380 K, a broadened peak is observed, which we fit to a single Gaussian peak. The temperature dependence of the FWHM is given in Fig. 10(c). The large FWHM indicates that the T phase is not LRO and instead consists of SRO regions. We speculate that these SRO tetragonal regions coexist in a cubic matrix around the Curie temperature. After cooling in an electric field $E = 1$ kV/cm, a well-defined LRO T phase is observed and manifested by the presence of tetragonal c domains along [001] and a domains along [100] (radial scans not shown in Fig. 10, but the lattice parameters are given in Fig. 9). Furthermore, recently a distinct tetragonal diffraction profile in the FC state with $E \parallel$ [001] was observed in a single crystal of the related relaxor ferroelectric system $\text{Pb}(\text{In}_{1/2}\text{Nb}_{1/2})\text{O}_3$ - $\text{Pb}(\text{Mg}_{1/3}\text{Nb}_{2/3})\text{O}_3$ - PbTiO_3 (PIN-PMN-PT) [29]. Short-range-ordered tetragonal regions may cluster together and grow into a conventional long-range-order phase under application of an E field [29].

Relaxor ferroelectric single crystals of PMN- x PT and PZN- x PT are known to possess a surface layer ~ 100 μm thick that is structurally distinct from the bulk, a phenomenon known as the anomalous skin effect [34,35]. The internal strains in these materials, which persist even after annealing at high temperature, will result in a d -spacing gradient that could produce a broadened and asymmetric x-ray diffraction profile [26,34,36]. Given that the absorption-limiting penetration depth ($1/e$) of Cu K_α x rays is about 2–3 μm in PZN- x PT [24], the most likely explanation for the asymmetric diffraction peak profiles in the cubic phase and the broad, T -like diffraction feature in the cubic matrix is the skin effect, as the low-energy x rays used here will scatter predominantly from the first one to two microns of the crystal surface. Even in the nonrelaxor materials SrTiO_3 and LaAlO_3 , a related skin effect has been reported, and a distinct symmetry observed between the near-surface region and the bulk [37,38]. Neutrons, by contrast, being charge-neutral particles, are able to penetrate far more deeply than x rays into crystals; they therefore provide structural information related to the average bulk crystal symmetry. Prior neutron studies have revealed symmetric peak profiles in the bulk of relaxor PZN- x PT crystals [39]. Hence the difference between neutron and x-ray diffraction profiles highlighted in this study provides evidence that the asymmetric peaks most likely result from this skin effect. Furthermore,

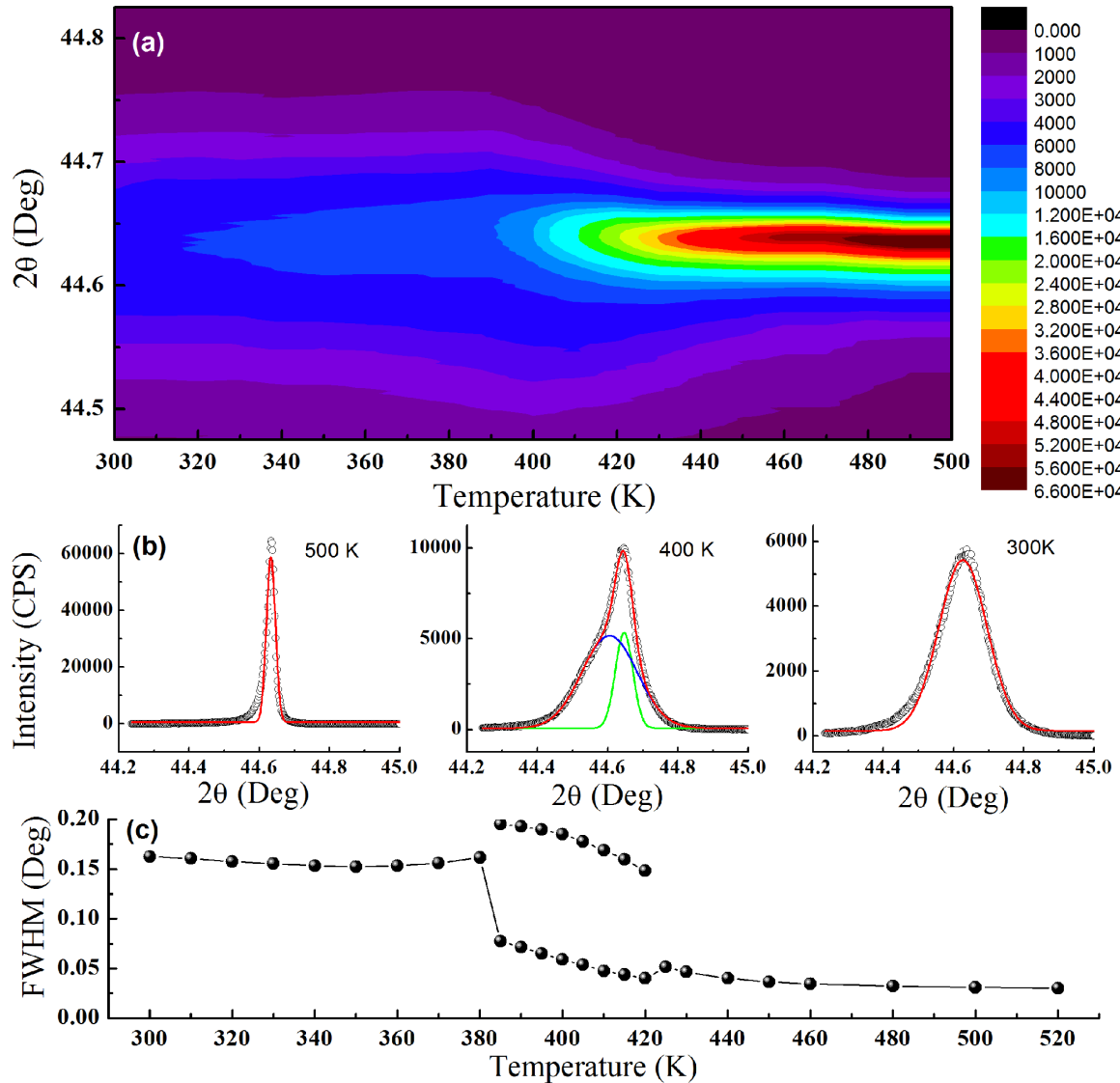


FIG. 10. (a) X-ray intensity contour map of the PZN-4.5%PT $(002)_C$ Bragg peak showing the evolution of the width with temperature. (b) Representative $(002)_C$ Bragg peaks at 500, 400, and 300 K. The data were fit using single-peak and two-peak Gaussian functions. (c) Temperature dependence of the $(002)_C$ Bragg peak FWHM derived from the Gaussian fits.

Ohwada *et al.* studied the c -axis lattice variation using both neutron and x-ray techniques during the R - M_A - M_C phase transition sequence, and they found a sharp jump in the c -axis lattice spacing using x rays that was not reproduced by neutron methods [36]. The difference between the diffraction features in the near-surface and bulk regions of the crystal suggests the presence of a nonuniform strain distribution within the skin. In the present study, even under an applied electric field E , we observe a notably asymmetric diffraction profile in both the high- and room-temperature phases, as shown in Fig. 6, which differs from the findings obtained from neutron diffraction. This is also consistent with the idea that the asymmetric diffraction profile is due to the skin effect.

In order to further elucidate the skin effect, additional diffraction measurements were made of $(200)_C$ Bragg peaks in single crystals of the conventional nonrelaxor ferroelectrics BaTiO_3 and PMN-60\%PT in the cubic phase, as the asymmetric peak broadening is a measure of the strain distribution

in the surface layer of relaxors [13,23,36]. The intensity of each diffraction peak is normalized to a value of 100, plotted on a linear scale, and shown in Fig. 11. From these data it can be seen that the size and strength of the diffraction peak asymmetry in the relaxors is much larger than that in nonrelaxor ferroelectric crystals. These findings demonstrate that the relaxor PZN-4.5%PT and PZN-6.5%PT crystals possess a significant skin effect.

PFM is an intrinsically surface-sensitive technique, so it cannot access the interior/bulk domain structure of relaxor crystals. Figure 12(a) shows an AFM image illustrating the surface roughness ($10\ \mu\text{m} \times 10\ \mu\text{m}$) for a PZN-4.5% crystal. Vertical PFM phase images were then acquired at 400, 430, and 450 K on heating, as shown in Figs. 12(b)–12(d). It is interesting to note that ferroelectric domain structural features, which weaken with increasing temperature, are seen that persist to several tens of degrees above the bulk Curie temperature. We note that similar observations have previously

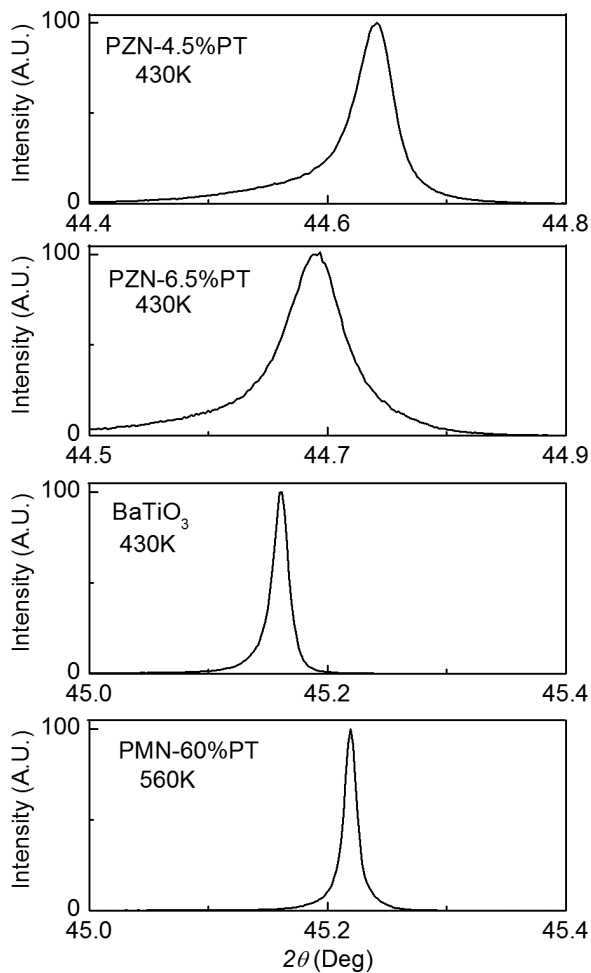


FIG. 11. Profile of the pseudocubic $(200)_C$ Bragg peak in the cubic phase for relaxor and normal ferroelectric single crystals: PZN-4.5%PT at 430 K, PZN-6.5%PT at 430 K, BaTiO_3 at 430 K, and PMN-60%PT at 570 K. The intensity of each diffraction peak was normalized in order to clearly reveal the asymmetric and broadened features.

been reported for PZN-12%PT [35]. Again, these features can be attributed to strain gradient distributions, unique atomic configurations, and/or a distinct stoichiometry of the surface layer [34,35,40].

Diffuse scattering, such as Huang scattering, could also give rise to asymmetric diffraction profiles [41]. However, we argue that diffuse scattering cannot be the cause of the asymmetric diffraction peak profiles observed in our study. In PZN- x PT, the diffuse scattering intensity is orders of magnitude weaker than the Bragg peak intensity, whereas in this study the asymmetry is visible even when the intensity is plotted on a linear scale (see Fig. 11). In addition, the reciprocal-space mesh scans (see Figs. 7 and 8, also plotted on linear scale) show no evidence of the well-known butterfly-shaped intensity contours around (200) or the elliptically shaped contours around (220) [42,43]. For these reasons, we believe that the skin effect is the most possible cause of the diffraction peak asymmetry in the cubic phase. The skin effect would also explain why the diffraction peaks broaden below the Curie temperature: Xu *et al.* showed that the size of the structural

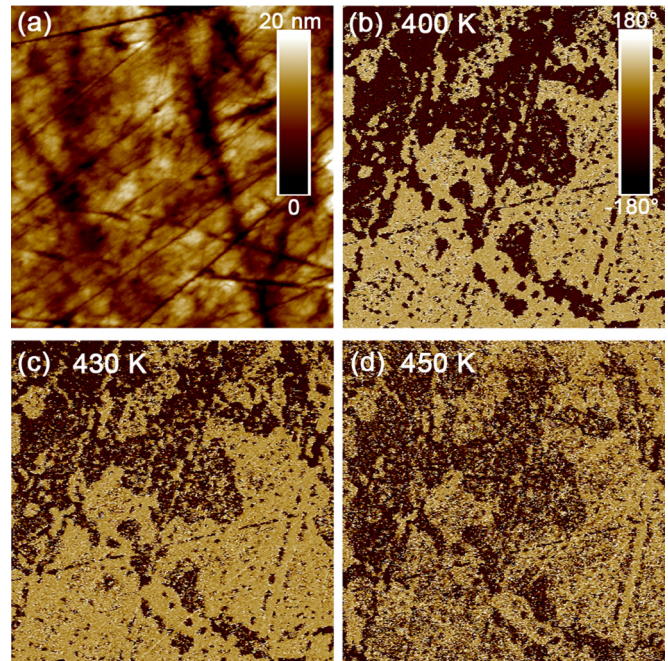


FIG. 12. (a) Topography AFM image of the surface roughness of PZN-4.5%PT single crystals of an area of $10 \times 10 \mu\text{m}$ and (b)–(d) the corresponding phase image of PFM of the same region at various temperatures. The surface ferroelectric domain configuration remains identical above the bulk phase transition.

distortion decreases with increasing distance from the crystal surface in PZN- x PT [25] and PZN [24]; thus the very-near surface region of the crystal never achieves long-range order.

2. Near the $C \rightarrow T$ phase transition region in the FC state

Broadened diffraction peaks are also notable in the vicinity of the $C \rightarrow T$ transition temperature, and are seen in transverse scans of the $(200)_T$ and $(220)_T$ Bragg peaks in PZN-6.5%PT, whereas that for $(002)_T$ exhibits a sharp peak profile, as shown in Figs. 8(a)–8(c). Similar profiles have also been observed in ternary PIN-PMN-PT relaxor crystals. In order to determine the underlying mechanism for this phenomenon, rocking curves (ω scans at fixed 2θ values) were performed around $(002)_T$, $(200)_T$, and $(220)_T$, as shown in Fig. 13, where one or more Gaussian functions were fit to each curve. The results show a single peak around $(002)_T$ and doublets around $(200)_T$ and $(220)_T$. The splitting along the *transverse direction* are similar to those found in the M_C phase under application of an electric field $E \parallel [001]$ [32]. However, the crystals are unambiguously in the T -phase region, as can be seen from radial scans and the evolution of the lattice parameters with temperature [see Fig. 9(b)]. The splitting of the rocking curves around the (200) and (220) peaks in the tetragonal region may be interpreted as evidence that the M_C phase is a “ferroelectric adaptive phase” [44–47]. Under the application of moderate electric fields along $[001]$, the polarization vectors of the tetragonal regions will tend to align with the E field; however, a fraction of the vectors may remain perpendicular: Thus, the domain state is referred to as a pseudo-monodomain configuration. Such polydomain ferroelastic crystals consist

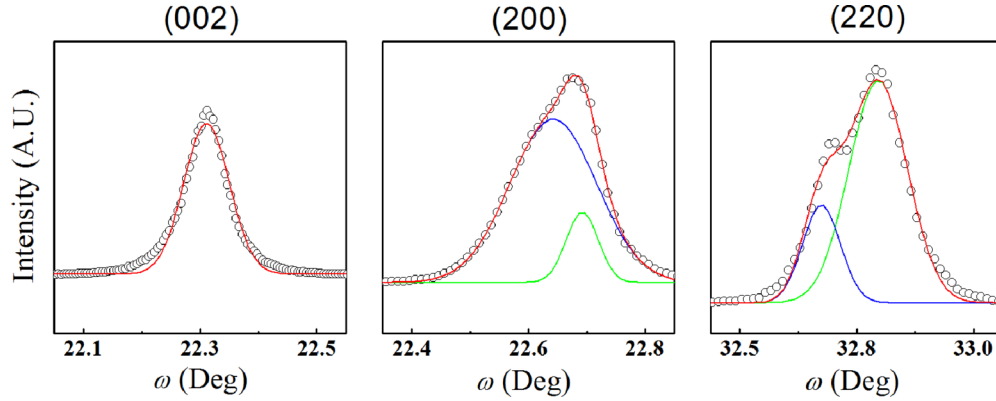


FIG. 13. Comparison of rocking curves for FC PZN-6.5%PT in the tetragonal phase.

of structural twins that accommodate elastic strain [45,48]. Wang has predicted that the twinned a and c domains in the T phase can produce a superlattice of M_C symmetry if they are adaptive [46,47]. In turn, this leads to a splitting in the ω scans along the $(200)_T$ and $(220)_T$ peaks, given as

$$\beta_C = 90^\circ + 2A\nu(1 - \nu) \left(\tan^{-1} \frac{c_t}{a_t} - 45^\circ \right), \quad (1)$$

where β_C is the angle of the low-symmetry M_C phase, A is a fitting constant (close to 1), and ν is the volume fraction of the twinned a or c domains. The diffraction broadening feature along the transverse direction in Fig. 8 may result from twin-related tetragonal nanovariants, not being perfectly stable with respect to each other in a manner that achieves complete stress accommodation. We note that this feature (i.e., diffraction broadening along the transverse direction) is more profound in a poled PIN-PMN-PT crystal [12], indicating poled relaxor crystals are dominated by nanotwins. These results also provide indirect evidence that the nanotwin boundary is the origin of high piezoelectric properties for relaxor ferroelectric crystals [48].

B. Crystal structure at 300 K

As shown in Fig. 4, the $(002)_C$ and $(200)_C$ Bragg peaks at 300 K are significantly different, much more so than in the high-temperature region. As a result, the difference between the a - and c -axis lattice parameters determined from the $(200)_C$ and $(002)_C$ peaks is notably larger than the experimental errors (see Fig. 5). These findings show that the ground state for PZN-4.5%PT is not a long-range-ordered R phase (nor is that for PZN-6.5%PT, data not shown). This is inconsistent with previous observations by single-crystal and powder diffraction, via low- and high-energy x-ray beams [6,25]. Our findings are similar to those for PZN-8%PT reported by Ohwada *et al.*, where an unknown ground state designated as “phase X ” was conjectured. Also puzzling is the difference between the peak intensities at $(200)_C$ and $(002)_C$ and whether or not this difference is intrinsic. The d spacings were determined by the positions of the diffraction peaks, which can be influenced by the surface condition [i.e., $(200)_C$ and $(002)_C$]: such as mechanically induced stain, defect, or stoichiometric inhomogeneity [23]. However, before each measurement, the crystals were annealed above 600 K for

30 min to relax the residual surface strain. Interestingly, the intensity and FWHM of the $(002)_C$ and $(200)_C$ peaks exhibited differences above the Curie temperature (see Fig. 4 at 430 K); this difference increased with decreasing temperature (i.e., as the c lattice increased, and the a lattice decreased).

In addition to the difference between the diffraction intensities at $(002)_C$ and $(200)_C$, the peak profiles were highly asymmetric, as can be seen from the one-peak Gaussian mode fits shown in Fig. 10(b). This asymmetry indicates that additional peaks may exist within the broad one, but were hard to distinguish. We note that the asymmetry of the $(200)_C$ peak is consistent in peak position ranges with the $(002)_C$ (see Fig. 4). We thus could speculate that the ground state might be a monoclinic phase, rather than the distorted cubic phase X as proposed by Ohwada *et al.*

The FWHM of the $(200)_C$ diffraction peak is much larger than expected given the resolution of the Ge (220) cut crystal analyzer [see Fig. 10(c)]. The large FWHM most likely results from a collection of microcrystal boundaries contributing to the total scattering intensity [26]. An explanation for this broadening nature has conventionally been a skin effect, which is known to effect x-ray studies of relaxor crystals due to the limited x-ray penetration depth [26]. The neutron study of both powder and single-crystal samples of PMN- x PT by Phelan *et al.* [13] has shown that the skin effect vanishes on the tetragonal side of the MPB, i.e., for Ti concentrations $x \sim 0.40$ and higher. They presented a revised PMN- x PT phase diagram where the ground state was designated as “short-range R/M ” [13]. Analogously, the ground state of PZN- x PT on the left side of the MPB was indexed as a SRO monoclinic structure because they share similarly broadened features. During a manuscript revision, Zhang *et al.* [10] found experimental evidence that a LRO R phase coexists with both LRO and SRO monoclinic regions on the Zr-rich side of the MPB of PZT. These findings indicate the ground state of these relaxor solid solutions may be more complex than previously thought.

C. Extension of the T phase region by E

It was found that the stability of the T phase is significantly enhanced by the application of an electric field E for single crystals of PZN- x PT with $x = 4.5\%$ and 6.5% , compositions that lie on the left side of the MPB. Even though PZN- x PT crystals with $x > 9\%$ (i.e., located on the right side of the

MPB) were not studied, one can make inferences from the related ternary PIN-PMN-PT relaxor solid crystals, located near the MPB but to the right (Ti-rich) side. In this case, an E -field-induced enhancement of the T -phase stability was clearly observed. We thus believe that this phenomenon is a common feature for all relaxor crystals, and not strongly dependent on compositions.

1. Extension of the T phase to higher temperatures

In order to understand the extension of the T phase to higher temperatures (T) by the application of an electric field E , a simple form of the classical Landau theory was employed. Generally, the free energy (G) of the system, being a function of the mole fraction PT (x) and T , can be described as a symmetry-adapted Landau series with respect to the absolute value of the spontaneous polarization P in the unconstrained state,

$$G(x, T, P) = \frac{1}{2}\alpha(x)(T - T_0)P^2 + \frac{1}{4}\beta(x)P^4 + \frac{1}{6}\gamma(x)P^6 - EP, \quad (2)$$

where $\alpha(x)$, $\beta(x)$, and $\gamma(x)$ are the coefficients of the various ordered terms, respectively. E is the normalized externally applied electric field, where it is also assumed that P and E are parallel.

Our idea is to determine, in the simplest possible case, the E -field-induced extension of the T phase. For a first-order phase transition, one can assume that $\alpha(x) > 0$, $\beta(x) < 0$, and $\gamma(x) > 0$. When $E = 0$, $G(P)$ has two minima at $P \neq 0$ in addition to one at $P = 0$. For $T < T_C$, $G < 0$, so that a discontinuous transition occurs from $P = 0$ into the state with two minima at $P \neq 0$. The paraelectric \rightarrow ferroelectric transition temperature T_C under $E = 0$ can then be found as

$$T_C = T_0 + \frac{3}{16} \frac{\beta(x)^2}{\alpha(x)\gamma(x)}. \quad (3)$$

From the Clausius-Clapeyron equation [$T_C(E) = T_C - \frac{\Delta P}{\Delta S} E$, where ΔP and ΔS are the discontinuous change in polarization and entropy at T_C], the Curie temperature T_C at various E is

$$T_C(E) = T_C + \frac{4}{\alpha(x)} \sqrt{\frac{-\gamma(x)}{3\beta(x)}} E. \quad (4)$$

From Eq. (4), it is obvious that T_C increases with increasing E field when $\alpha(x) > 0$. This prediction that the T phase is extended by E applied parallel to [001] is a common characteristic of all $T \rightarrow C$ transitions that are first order, independent of the composition and the category of the crystals.

2. Extension of the T phase to lower x

As shown in Fig. 4, the coexistence of T and C phases was only found for PZN-4.5%PT crystals in the ZFC state, where a $C \rightarrow$ SRO monoclinic transformation occurred on cooling. However, for [001] PZN-4.5%PT crystals in the FC state, the T phase existed independently of C (see Fig. 6). This demonstrates that the T phase can be extended to lower-PT contents under E .

In the PZN- x PT solution, substitution of the $[\text{TiO}_4]^{4-}$ octahedron for the more complex $[\text{Zn}_{1/2}\text{Nb}_{2/3}\text{O}_4]^{4-}$ results in an MPB separating R and T ferroelectric phases. The c/a ratio of the T phase weakens with decreasing x on approaching the MPB. PZN-4.5%PT can be considered as a special composition in the diagram, where a gradual transition between T microdomains in a C matrix and a macroscopic T phase begins to occur. If the T microdomains are much smaller than the coherence length of the x rays, then the average structure will appear monoclinic in the ZFC state. However, in the FC state the T microdomains align parallel to E , and thus a macroscopic T phase is observed on cooling in between the C and M_A phases.

D. Destruction of the old and creation of another MPB by field cooling

The most significant feature in Fig. 1 is the destruction of the R/M and T MPB of the ZFC state, by applying a moderate E , and creating another one. PZN-4.5%PT and PZN-6.5%PT undergo a transformational sequence $C \rightarrow T \rightarrow M_C \rightarrow M_A$. This sequence is similar to that previously reported for PZN-8PT by Ohwada *et al.*, except the present results reveal that the $M_C \rightarrow M_A$ transition is decreased to room temperature by field cooling.

In the ZFC state, the transformational sequence is $C \rightarrow T \rightarrow R$ or M for $x < 8\%$, while the transformational sequence is $C \rightarrow T$ for $x > 11\%$. In the ZFC state, a MPB exists for $8\% < x < 11\%$, which is nearly vertical separating R or M and T phases. However, under $E \parallel [001]$, a bridging M_C phase is found near the MPB, and in particular, the vertical nature of the MPB was transformed in the x - T field to being notably bent towards the lower- x side. This M_C phase appeared not only in the range of the MPB of the ZFC state of $8\% < x < 11\%$, but also over an extended range of $4.5\% < x < 8\%$. To understand the tilting of the MPB, it is worth referring to the polarization rotation path of PZN- x PT for $E \parallel [001]$ as the polarization rotation path depends on x . The bifurcated path indicates that the lowest free-energy path for the various compositions is different. Analogously, we conjecture that the lowest free-energy path is also different in the cooling process without (i.e., ZFC state) and with (i.e., FC state) an E field applied to a constant composition, and for different compositions in the FC state. For PZN-6.5%PT, the polarization rotation path is along $T \rightarrow R$ in the ZFC state, while in the FC state, the polarization first rotates along the $T \rightarrow O$ path, and then abruptly jumps to the $T \rightarrow R$ one. This results in a modified phase transition sequence of $T \rightarrow M_C \rightarrow M_A$, whereas, for low-PT crystals (i.e., $x < 4.5\%$), the polarization rotation path is along $T \rightarrow R$ in both ZFC and FC (e.g., moderate amplitude of $E = 1$ kV/cm) states.

E. Atypical M_C domain configurations in FC PZN-6.5%PT

Monoclinic symmetry allows for 24 possible domain states and thus normally results in very complicated domain configurations. However, in PMN-PT and PZN-PT crystals, an applied $E \parallel [001]$ fixes the c axis, simplifying the configuration. The resultant signature polar vector orientation and domain configuration for the M_C phase are schematically illustrated in

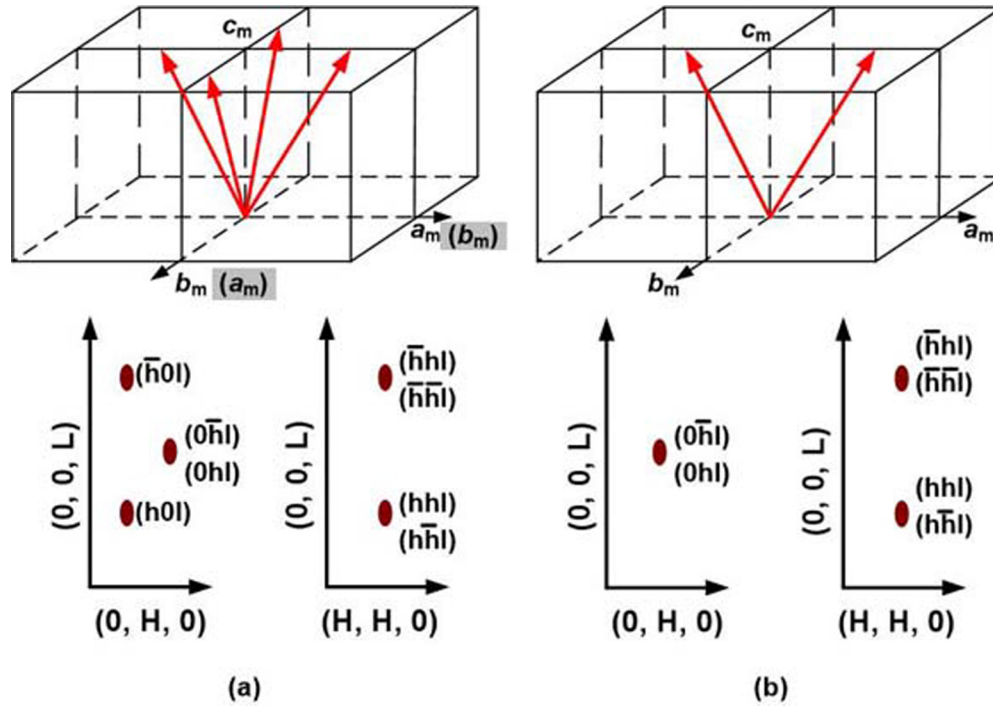


FIG. 14. Polar vectors and domain configurations in cubic Cartesian coordinates for the (a) signature M_C phase and (b) atypical M_C phase observed in this work. The polar vector in the monoclinic M_C phase lies in the $a_m - c_m$ monoclinic plane, as designated by the arrows.

Fig. 14(a). In the HOL plane, there are only two b domains that are related by a 90° rotation about the c axis, where each of these has two related a domains having an angle of β or $180-\beta$ with c_m . The polarization vectors of each of these four domains is rotated under E in the monoclinic plane, forming identical angles along the $[001]$.

An atypical domain configuration was observed in this experiment as shown in Fig. 8 and schematically illustrated in Fig. 14(b). As expected, a single peak was observed around the (002) zone, illustrating that the c axis is fixed along the direction that E was applied. However, about the (020) zone, only a single b domain was found that was slightly tilted along the longitudinal direction, rather than containing two a domains in a typical case. Generally, in the M_C phase, the a and b domains can be switched between each other about the c axis, as designated by shaded and unshaded axis labels in Fig. 14(a). In turn, four polar vectors in the $a_m c_m$ plane are possible. However, surface residual stress in the ferroelectric crystals can break this domain equivalence, resulting in some domains being absent compared to the equilibrium configuration.

V. CONCLUSIONS

A comprehensive x-ray diffraction study of single-crystal PZN-4.5%PT and PZN-6.5%PT was performed on cooling under $E = 0, 1,$ and 2 kV/cm. In the ZFC state, the ground-state crystal structure of PZN-4.5%PT resembles a short-range-ordered monoclinic phase or a distorted rhombohedral one due to the skin effect, which is consistent with a previous synchrotron study by Xu *et al.* on the same compound [24]. It was established that the phase transformational sequence

with decreasing temperature for both PZN-4.5%PT and PZN-6.5%PT is $C \rightarrow T \rightarrow M_C \rightarrow M_A$ in the FC state. An $[001]$ FC phase diagram was constructed based on these diffraction data, and it was found that the phase stability and MPB were fragile to application of moderate electric fields. The T -phase region was found to be significantly extended by E . In particular, the vertical nature of the MPB in the ZFC diagram was lost.

ACKNOWLEDGMENTS

The work at Nanjing University of Science and Technology was supported by the National Natural Science Foundation of China (Grants No. 51602156 and No. 11134004), the Natural Science Foundation of Jiangsu Province, China (Grant No. BK20160824), the Fundamental Research Funds for the Central Universities (Grants No. 30916011208 and No. 30916011104), and the Opening Project of Key Laboratory of Inorganic function material and device, Chinese Academy of Sciences (Grant No. KLIFMD-2015-01). The US part of this collaborative work was sponsored by the Office of Naval Research (Grant No. N00014-13-1-0049). F.X. is thankful for the support from the Jiangsu Natural Science Foundation for Distinguished Young Scholars (Grant No. BK20140035). Y.W. thanks Dr. Z. G. Wang and C. T. Luo for the discussion. Certain commercial equipment or instruments are identified in this paper to foster understanding. Such identification does not imply recommendation or endorsement by the National Institute of Standards and Technology, nor does it imply that the materials or equipment identified are necessarily the best available for the purpose.

- [1] H. X. Fu and R. E. Cohen, *Nature* **403**, 281 (2000).
- [2] S. E. Park and T. R. ShROUT, *J. Appl. Phys.* **82**, 1804 (1997).
- [3] Y. Wang, J. Li, and D. Viehland, *Mater. Today* **17**, 269 (2014).
- [4] D. S. Paik, S. E. Park, S. Wada, S. F. Liu, and T. R. ShROUT, *J. Appl. Phys.* **85**, 1080 (1999).
- [5] B. Noheda, D. E. Cox, G. Shirane, J. Gao, and Z. G. Ye, *Phys. Rev. B* **66**, 054104 (2002).
- [6] D. La-Orautapong, B. Noheda, Z. G. Ye, P. M. Gehring, J. Toulouse, D. E. Cox, and G. Shirane, *Phys. Rev. B* **65**, 144101 (2002).
- [7] D. Phelan, X. Long, Y. Xie, Z. G. Ye, A. M. Glazer, H. Yokota, P. A. Thomas, and P. M. Gehring, *Phys. Rev. Lett.* **105**, 207601 (2010).
- [8] D. E. Cox, B. Noheda, G. Shirane, Y. Uesu, K. Fujishiro, and Y. Yamada, *Appl. Phys. Lett.* **79**, 400 (2001).
- [9] B. Noheda and D. E. Cox, *Phase Trans.* **79**, 5 (2006).
- [10] N. Zhang, H. Yokota, A. M. Glazer, Z. Ren, D. A. Keen, D. S. Keeble, P. A. Thomas, and Z. G. Ye, *Nat. Commun.* **5**, 5231 (2014).
- [11] B. Noheda, D. E. Cox, G. Shirane, R. Guo, B. Jones, and L. E. Cross, *Phys. Rev. B* **63**, 014103 (2001).
- [12] Y. Wang, Z. Wang, W. Ge, C. Luo, J. Li, D. Viehland, J. Chen, and H. Luo, *Phys. Rev. B* **90**, 134107 (2014).
- [13] D. Phelan, E. E. Rodriguez, J. Gao, Y. Bing, Z. G. Ye, Q. Huang, J. Wen, G. Xu, C. Stock, M. Matsuura, and P. M. Gehring, *Phase Trans.* **88**, 283 (2015).
- [14] B. Jaffe, W. R. Cook, and H. Jaffe, *Piezoelectric Ceramics* (Academic Press, London, 1971).
- [15] Y. Uesu, M. Matsuda, Y. Yamada, K. Fujishiro, D. E. Cox, B. Noheda, and G. Shirane, *J. Phys. Soc. Jpn.* **71**, 960 (2002).
- [16] B. Noheda, D. E. Cox, G. Shirane, J. A. Gonzalo, L. E. Cross, and S. E. Park, *Appl. Phys. Lett.* **74**, 2059 (1999).
- [17] A. A. Bokov and Z. G. Ye, *Appl. Phys. Lett.* **92**, 082901 (2008).
- [18] C. Ma, H. Guo, S. P. Beckman, and X. Tan, *Phys. Rev. Lett.* **109**, 107602 (2012).
- [19] H. Cao, J. F. Li, D. Viehland, and G. Y. Xu, *Phys. Rev. B* **73**, 184110 (2006).
- [20] K. Ohwada, K. Hirota, P. W. Rehrig, Y. Fujii, and G. Shirane, *Phys. Rev. B* **67**, 094111 (2003).
- [21] B. Noheda, Z. Zhong, D. E. Cox, G. Shirane, S. E. Park, and P. Rehrig, *Phys. Rev. B* **65**, 224101 (2002).
- [22] J. Kuwata, K. Uchino, and S. Nomura, *Ferroelectrics* **37**, 579 (1981).
- [23] W. S. Chang, M. Shanthi, K. K. Rajan, L. C. Lim, F. T. Wang, C. T. Tseng, C. S. Tu, P. Yang, and H. O. Moser, *J. Appl. Phys.* **101**, 124104 (2007).
- [24] G. Y. Xu, Z. Zhong, Y. Bing, Z. G. Ye, C. Stock, and G. Shirane, *Phys. Rev. B* **67**, 104102 (2003).
- [25] G. Y. Xu, H. Hiraka, G. Shirane, and K. Ohwada, *Appl. Phys. Lett.* **84**, 3975 (2004).
- [26] G. Y. Xu, D. Viehland, J. F. Li, P. M. Gehring, and G. Shirane, *Phys. Rev. B* **68**, 212410 (2003).
- [27] W. Ge, C. P. Devreugd, D. Phelan, Q. Zhang, M. Ahart, J. Li, H. Luo, L. A. Boatner, D. Viehland, and P. M. Gehring, *Phys. Rev. B* **88**, 174115 (2013).
- [28] K. H. Conlon, H. Luo, D. Viehland, J. F. Li, T. Whan, J. H. Fox, C. Stock, and G. Shirane, *Phys. Rev. B* **70**, 172204 (2004).
- [29] C. Luo, Y. Wang, Z. Wang, W. Ge, J. Li, H. Luo, and D. Viehland, *Appl. Phys. Lett.* **105**, 232901 (2014).
- [30] P. M. Gehring, W. Chen, Z. G. Ye, and G. Shirane, *J. Phys.: Condens. Matter* **16**, 7113 (2004).
- [31] A. Lebon, H. Dammak, G. Calvarin, and I. O. Ahmedou, *J. Phys.: Condens. Matter* **14**, 7035 (2002).
- [32] F. M. Bai, N. G. Wang, J. F. Li, D. Viehland, P. M. Gehring, G. Y. Xu, and G. Shirane, *J. Appl. Phys.* **96**, 1620 (2004).
- [33] H. Cao, J. Li, and D. Viehland, *J. Appl. Phys.* **100**, 034110 (2006).
- [34] G. Xu, P. M. Gehring, C. Stock, and K. Conlon, *Phase Trans.* **79**, 135 (2006).
- [35] N. Domingo, N. Bagues, J. Santiso, and G. Catalan, *Phys. Rev. B* **91**, 094111 (2015).
- [36] K. Ohwada, K. Hirota, P. W. Rehrig, P. M. Gehring, B. Noheda, Y. Fujii, S. E. E. Park, and G. Shirane, *J. Phys. Soc. Jpn.* **70**, 2778 (2001).
- [37] C. Jutta and E. K. H. Salje, *J. Phys.: Condens. Matter* **10**, 2817 (1998).
- [38] E. K. H. Salje, M. Alexe, S. Kustov, M. C. Weber, J. Schiemer, G. F. Nataf, and J. Kreisel, *Sci Rep.* **6**, 27193 (2016).
- [39] P. M. Gehring, K. Ohwada, and G. Shirane, *Phys. Rev. B* **70**, 014110 (2004).
- [40] P. Gao, H. J. Liu, Y. L. Huang, Y. H. Chu, R. Ishikawa, B. Feng, Y. Jiang, N. Shibata, E. G. Wang, and Y. Ikuhara, *Nat. Commun.* **7**, 11318 (2016).
- [41] H. You and Q. M. Zhang, *Phys. Rev. Lett.* **79**, 3950 (1997).
- [42] G. Y. Xu, P. M. Gehring, and G. Shirane, *Phys. Rev. B* **72**, 214106 (2005).
- [43] G. Y. Xu, Z. Zhong, Y. Bing, Z. G. Ye, and G. Shirane, *Nat. Mater.* **5**, 134 (2006).
- [44] D. Viehland, *J. Appl. Phys.* **88**, 4794 (2000).
- [45] Y. M. Jin, Y. U. Wang, A. G. Khachatryan, J. F. Li, and D. Viehland, *Phys. Rev. Lett.* **91**, 197601 (2003).
- [46] Y. U. Wang, *Phys. Rev. B* **74**, 104109 (2006).
- [47] Y. U. Wang, *Phys. Rev. B* **73**, 014113 (2006).
- [48] D. D. Viehland and E. K. H. Salje, *Adv. Phys.* **63**, 267 (2014).